Fabrication of Fully Inkjet-Printed Vias and SIW Structures on Thick Polymer Substrates

Sangkil Kim, *Member, IEEE*, Atif Shamim, *Senior Member, IEEE*, Apostolos Georgiadis, *Senior Member, IEEE*, Hervé Aubert, *Senior Member, IEEE*, and Manos M. Tentzeris, *Fellow, IEEE*

***Abstract*— In this paper, a novel fully inkjet-printed via fabrication technology and various inkjet-printed substrate-integrated waveguide (SIW) structures on thick polymer substrates are presented. The electrical properties of polymethyl methacrylate (PMMA) are thoroughly studied up to 8 GHz utilizing the T-resonator method, and inkjet-printable silver nanoparticle ink on PMMA is characterized. A long via fabrication process up to 1 mm utilizing inkjet-printing technology is demonstrated, and its characteristics are presented for the first time. The inkjet-printed vias on 0.8-mm-thick substrate have a resistance of ~0.2 Ω. An equivalent circuit model of the inkjet-printed stepped vias is also discussed. An inkjet-printed microstrip-to-SIW interconnect and an SIW cavity resonator utilizing the proposed inkjet-printed via fabrication process are also presented. The design of the components and the fabrication steps are discussed, and the measured performances over the microwave frequency range of the prototypes are presented.**

***Index Terms*— Additive fabrication, inkjet-printed substrate-integrated waveguide (SIW), inkjet-printed via, low-cost via fabrication, polymethyl methacrylate (PMMA).**

I. Introduction

INKJET-PRINTING technology is investigated and widely utilized as an alternative fabrication method to the conventional subtractive fabrication methods, such as milling and etching. The importance of green, scalable, and cost-efficient technology is ever increasing for numerous applications, such as the Internet of Things (IoT), the radio frequency identification (RFID) tags, and the wireless sensor networks [1]–[3]. The inkjet-printing technology does not produce any byproducts, because it only deposits the controlled amount of functionalized inks, such as silver nanoparticles on desired position. In addition, it is a completely dry process, which is compatible with most modern fabrication processes [4]. Arbitrary geometries with small feature sizes (<50 μm) can be printed on numerous substrates without any special masking [5]–[7]. Recently, the development of various types of nanoparticle-based inks, such as polymers, carbon nanotubes, piezoelectric materials, and high dielectric constant materials, has attracted significant interest from many researchers [8]–[11]. Numerous studies and applications utilizing inkjet-printing technology in microwave area have been reported, including inkjet-printed wireless power transfer topologies, RFID-based sensors, and microwave components for high-speed communication systems [12], [13]. However, most of these works are single-layered structures, because it is challenging to realize the inkjet-printed vias, which are one of the most critical factors for the realization of highly integrated systems, packages, and multilayered structures.

In this paper, the implementation of inkjet-printed stepped vias on thick substrates (thickness $>$ 100 μm) is presented for the first time. Only a small number of technologies for implementing vias utilizing the inkjet-printing technology have been reported, all of which have been implemented on thin substrates with thickness below 100 μm [14]–[18]. Such thin substrates are unsuitable for applications in relatively lower frequency bands, such as mobile, WiFi, Industrial, Scientific, and Medical, and so on. The feature size of microwave components, such as the width of microstrip line, is narrow on thin substrate, which results in high design sensitivities to fabrication tolerances. On the other side, the radiation efficiency of antennas, such as patches, resonators, and waveguide structures [such as substrate-integrated waveguides (SIWs)], is significantly affected by the substrate thickness [19]. Therefore, it is necessary to develop via fabrication concepts or techniques, which can be applied to various substrates of different thicknesses. The major issue in the metallization of via holes utilizing the inkjet-printing technology is to maintain a continuous and uniform metal layer, since the printed traces shrink after the sintering process, which is challenging because the inkjet-printed silver nanoparticles shrink during the sintering process. Cylindrical copper pillars were inserted in laser-drilled via holes to metalize the thick via holes [20]. High conductivity and thick metal thickness compared with those of the printed nanoparticle-based metallic layers can be achieved by using this technology, since thick copper pillars are utilized. However, it has limited design degrees of freedom because the size of copper pillar

Manuscript received July 19, 2015; accepted January 7, 2016. Date of publication February 10, 2016; date of current version March 10, 2016. The work of S. Kim and M. Tentzeris was supported by NSF and DTRA. The work of A. Georgiadis has been supported by the EU COST Action IC1301 WiPE Wireless Power Transmission for Sustainable Electronics, the Generalitat de Catalunya under Grant 2014 SGR 1551 and by EU H2020 Marie Sklodowska-Curie grant agreement No 661621. Recommended for publication by Associate Editor A. Shapiro upon evaluation of reviewers' comments.

S. Kim is with Qualcomm, San Diego, CA 92121 USA (e-mail: zergling1023@gmail.com).

A. Shamim is with the King Abdullah University of Science and Technology, Thuwal 23955-6900, Saudi Arabia (e-mail: atif.shamim@kaust.edu.sa).

A. Georgiadis is with the Centre Tecnologic de Telecomunicacions de Catalunya, Barcelona 08860, Spain (e-mail: ageorgiadis@cttc.es).

H. Aubert is with the Laboratory for the Analysis and Architecture of Systems, National Center for Scientific Research, Micro and Nanosystems for Wireless Communications Research Group, Toulouse 31400, France (e-mail: haubert@laas.fr).

M. M. Tentzeris is with the School of Electrical and Computer Engineering, Georgia Institute of Technology, Atlanta, GA 30332 USA (e-mail: etentze@ece.gatech.edu).

Color versions of one or more of the figures in this paper are available online at http://ieeexplore.ieee.org.

Digital Object Identifier 10.1109/TCPMT.2016.2522461

(i.e., length, radius, and so on) is fixed, and an additional soldering process is required to ensure the contact between the planar metallic layers and the copper vias.

In this paper, a novel via hole topology with an exponentially tapered profile is introduced in order to facilitate the formation of continuous metal layers using conductive inks. As a proof-of-concept demonstration of the proposed inkjet-printed stepped-via configuration, an equivalent circuit model and an SIW structure, such as a microstrip-to-SIW transition, are presented on the polymethyl methacrylate (PMMA) substrate. A via array and an SIW cavity resonator are also presented on RT/Duroid 5880 to verify the repeatability of the via fabrication process and its performance. SIW structures require a large number of vias, which make them good benchmarking structures to test the repeatability and the performance of the proposed stepped vias. PMMA, which is also known as Plexiglas or acrylic, is a widely used commercial polymer material for numerous applications, such as display devices and medical instruments, due to its high transparency and good compatibility with human tissues [21]. However, the electrical properties of PMMA at microwave frequency range as well as the characteristics of inkjet-printed silver nanoparticles on PMMA are not well known. Therefore, PMMA is chosen as a substrate, and its electrical properties are characterized for the first time in this paper. In addition, the demonstration of the first fully inkjet-printed SIW structures suggests the importance of inkjet-printing technology toward implementing the system-on-substrate concept in communication, sensing, and IoT applications [13], [19].

In Section II, the characterization of PMMA and inkjet-printed silver nanoparticles on PMMA is presented, while in Section III, the fabrication process of inkjet-printed stepped via is introduced. Section IV introduces the first fully inkjet-printed SIW structures, including an SIW cavity resonator and a microstrip-to-SIW transition.

II. Inkjet-Printing Process on PMMA Substrate

PMMA was chosen as the substrate for the realization of the via-enabled structures in this paper, because its electrical properties at microwave frequency range were not clearly reported although it is widely utilized for microwave applications, such as in microfluidic sensors. A thorough characterization of the inkjet-printed silver nanoparticles on PMMA is necessary in order to extend the capabilities of inkjet-printed technologies to include via metallization and fabrication of SIW topologies.

In this section, the properties (conductivity and thickness) of inkjet-printed conductive traces using silver nanoparticles on PMMA substrate are investigated, while the electrical properties of PMMA are characterized within the microwave frequency range (1∼8 GHz) utilizing the T-resonator method [22].

A. Inkjet-Printed Silver Nanoparticles on PMMA

The properties of inkjet-printed silver nanoparticles have different values depending on the substrate properties. It is because different substrates have different physical surface properties, such as roughness, surface energy, and contact angle with the ink, that result in different inkjet-printability and printing challenges [23].

Simple rectangular traces (0.5 mm × 5 mm) were printed on PMMA substrate (Goodfellow, London, U.K. [24]) in order to investigate the properties of inkjet-printed silver nanoparticles on PMMA. The DMP2800 inkjet printer was utilized to print silver nanoparticles in this paper. For printing, the Dimatix 10-pL cartridge (DMC-11610) was used, and it was kept at a distance of 250 μm from the surface of the substrate. The printer head angle was 4.5°, which achieves a printing resolution of 1270 dpi. Cabot conductive ink CCI-300 was jetted at a nozzle temperature of 36 °C, while the substrate was maintained at room temperature (25 °C). Fig. 1(a) shows the thickness of the printed silver nanoparticle-based lines depending on the number of printed layers. The printed patterns were sintered at 120 °C for 2 h, and the thickness was measured using a Veeco Dektak 150 surface profilometer. Each printed layer added about 500 nm of thickness to the printed traces. A reported minimum feature size of the silver nanoparticle ink using a commercially available printer is ∼50 μm up to five layers of printing. After printing the third layer, the coffee ring effect has been observed because of the high surface energy of PMMA. The high surface energy of PMMA results in different drying speeds of ink at the edge and middle of the printed patterns [25], [26]. The width of the printed trace is additionally increased by ∼80 μm for each additional printed layer when the thickness (height) of the printed traces has exceeded 1.5 μm. The inkjet-printing technology is a thin metal process that the thickness of printed traces, such as metals and polymers, is about one skin depth or less at the microwave frequency range. However, it takes the advantage of flexibility, ease of fabrication, and cost efficiency of the printing technology, which are the critical properties for implementing novel applications, such as IoT. The conductivity (σ) of the inkjet-printed silver nanoparticles was also extracted using the measured profiles of the printed traces using

$$\sigma = \frac{l}{R \cdot A} \text{ (S/m)} \tag{1}$$

where l is the length of the trace, R is the resistance across the trace, and A is the cross section area of the trace. The cross section areas of the printed traces were numerically integrated over the line width [Fig. 1(a)]. Fig. 1(b) shows the extracted conductivities for different sintering temperatures as a function of the number of printed layers. The conductivity value converges after printing three layers, because the particle density is saturated. Higher sintering temperatures resulted in higher conductivity values, as reported in [13] and [27]. The converged conductivity values of the silver nanoparticle ink were around 4.4×10^6 S/m at 120 °C, 5.7×10^6 S/m at 150 °C, and 6.9×10^6 S/m at 180 °C. It corresponds to 6.98%, 9.05%, and 10.95% of bulk silver's conductivity ($\sigma_{\text{Ag}} = 6.3 \times 10^7$ S/m), respectively.

B. RF Characterization of PMMA

A commercially available PMMA sample has been characterized up to 8 GHz through the microstrip T-resonator

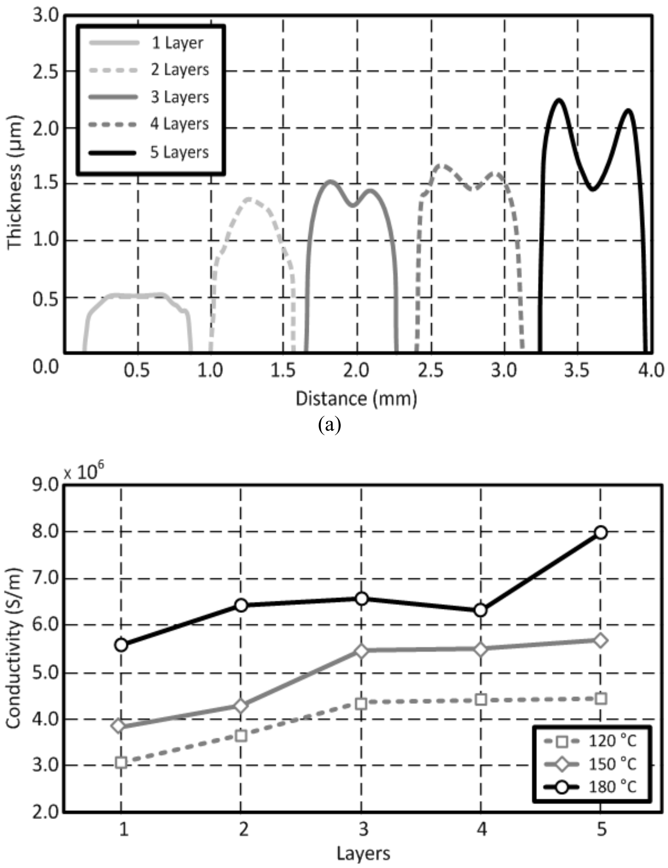

(a)

(b)

Fig. 1. Thickness and conductivity of inkjet-printed traces. (a) Thickness. (b) Conductivity.

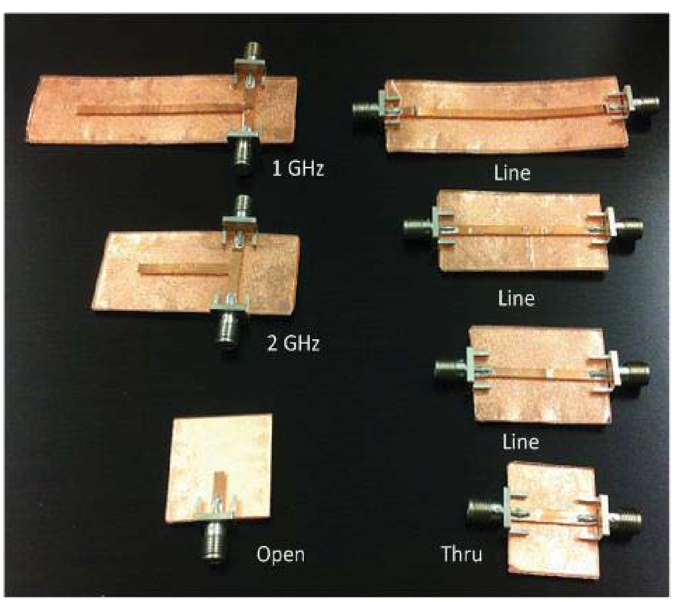

Fig. 2. Fabricated T-resonators and TRL calibration lines on PMMA substrate.

method in this paper. The relative permittivity (ε_r) and the loss tangent ($\tan\,\delta$) have been extracted from the measurements. Fig. 2 shows the fabricated T-resonator structures and the

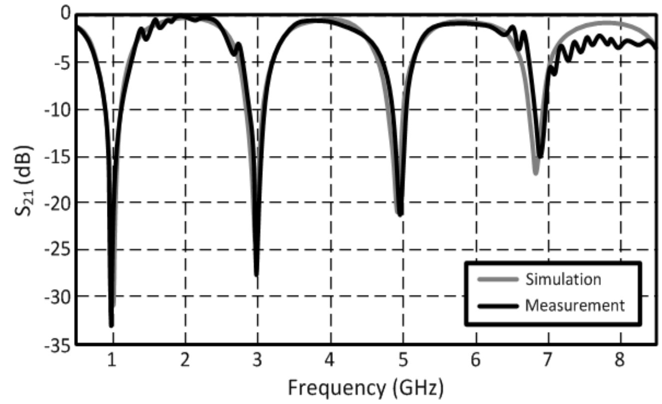

Fig. 3. S_{21} of the 1-GHz T-resonator.

thru-reflection-line (TRL) calibration structures on 1-mm-thick PMMA. The T-resonators consist of 50-Ω feeding lines and an open stub. The length of the open stub is quarter-wavelength ($\lambda_g/4$) at the desired resonant frequency. The width of the microstrip feeding lines was 2.8 mm, and the length of the T-resonator for 1 GHz is 51.92 mm and for 2 GHz is 25.56 mm. Fig. 3 shows the measured S_{21} of the fabricated T-resonator for 1 GHz. The measurement and simulation results are in good agreement. The resonant frequencies (f_n) of the T-resonator can be determined by

$$f_n = \frac{n \cdot c}{4(L_{\text{phy}} + L_O - L_T)\sqrt{\varepsilon_{\text{eff}}}} \tag{2}$$

where n is the odd resonance mode order ($n = 1, 3, 5 \ldots$), c is the speed of light in free space, L_{phy} is the physical length of the open stub, L_O is the correction factor for the open-end effect of the open stub, L_T is the correction factor for the T-junction effect, and ε_{eff} is the relative effective permittivity [22].

The loss tangent ($\tan\,\delta$) of the PMMA substrate was extracted from the quality factor (Q) of each resonance, as reported in [22]. The conductor losses were theoretically estimated using the equations reported in [30], and the radiation losses were also theoretically calculated utilizing 3-D full wave simulator, ANSYS High Frequency Structural Simulator (HFSS) v11.1.1. A thin copper sheet (thickness = 100 μm and $\sigma = 5.8 \times 10^7$ S/m) was utilized as the metal layer.

The coaxial SubMiniature version A (SMA) connectors were mounted using a conductive silver epoxy, and TRL calibration was applied to deembed the effects of feeding lines and the SMA connectors. The extracted effective permittivity (ε_{eff}) was converted into relative permittivity (ε_r). The resulting relative permittivity (ε_r) was 2.38 $\pm$ 0.12, and the extracted $\tan\,\delta$ was 0.011 $\pm$ 0.002 over the frequency of 1$\sim$8 GHz band, as shown in Fig. 4. The error intervals were estimated for a 99% confidence interval. Characterization results using the two-line-method are included in Fig. 4 for validation purpose [32]. Two transmission lines with the same characteristic impedance and two different lengths (20 and 70 mm) were prepared on the same substrate, and their scattering parameters (S_{21}) were measured. The lengths of the transmission lines were corresponding to effective

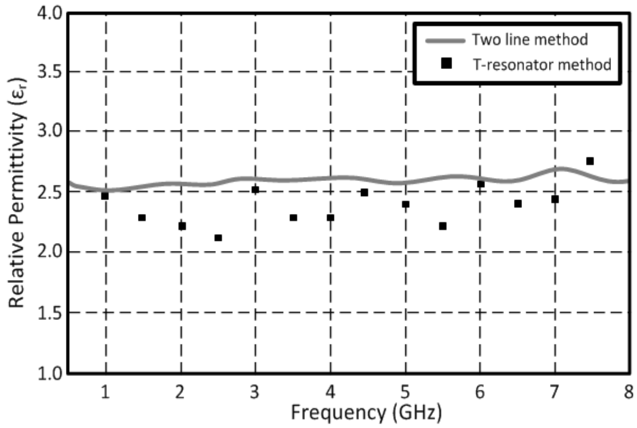

(a)

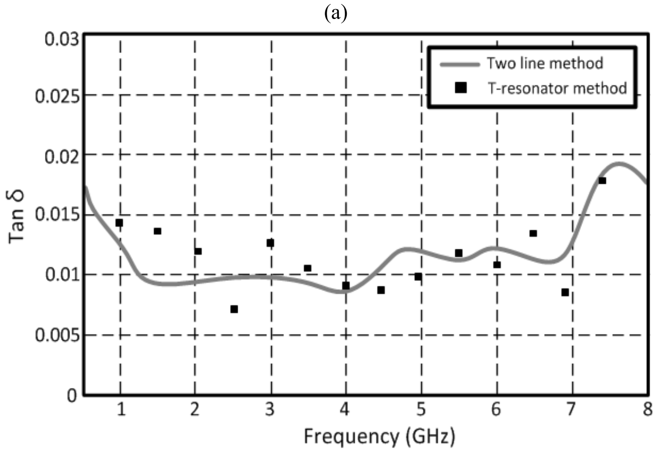

(b)

Fig. 4. Extracted (a) relative permittivity (ε_r) and (b) loss tangent (tan δ).

electrical length of 30° and 100° at 1 GHz, respectively. These transmission lines were utilized as the delay lines for TRL calibration. The relative dielectric constants (ε_r) over the frequency range of operation were extracted from the phase difference of the test transmission lines, and the values of tan δ over the frequency were calculated from the attenuation constant (α) of the transmission lines. The calculated radiation loss using 3-D electromagnetic simulator of the transmission line was subtracted from the measurement. These results are in good agreement and support the extracted values from the T-resonator method. The extracted dielectric constant values from the T-resonators vary compared with the values from the transmission line method. It is because of the fabrication error of each resonator, since the T-resonators were cut out from a copper tape. However, the extracted values from each resonators, such as a T-resonator for 1 GHz (resonant frequencies: 1, 3, 5, and 7 GHz), are robust over the frequency band.

III. Inkjet-Printed via

In this section, a novel via fabrication process on thick substrates utilizing the inkjet-printing technology is presented. In previously reported research efforts, inkjet-printed via holes have been successfully implemented on thin substrates [14]–[18], as shown in Table I. In [14], the three layers of silver nanoparticles have been printed over a thin vertical wall utilizing 50-pL cartridge. In [15], a craterlike via hole is made by inkjet printing an ethanol drop to dissolve a polyvinyl phenol layer. In [16], a microvia array, which consists of small laser-drilled microvias, is presented on polyimide substrate. In [17] and [18], the printed microwave structures, such as microstrip lines, are presented, and the reported loss of printed microstrip lines is about 0.3~0.5 dB/mm up to 10 GHz. The reported printed vias shown in [14]–[18] are built on a thin substrate, whose thickness is <100 μm. The proposed stepped-via approach (with a 2-mm diameter) achieved the via thickness of 800~1000 μm with a good via resistance of 0.2 Ω compared with the reported works.

TABLE I
Via Comparison

	Via thickness (μm)	Via diameter (μm)	Resistance (Ω)
[14]	25 ~ 65	N/A	1.9 ± 0.1
[15]	0.5	0.75	5×10^5
[16]	100	65	0.52
[17][18]	50 ~ 80	N/A	0.073 ± 0.043
Proposed Structure	800 ~ 1000	2000	0.2

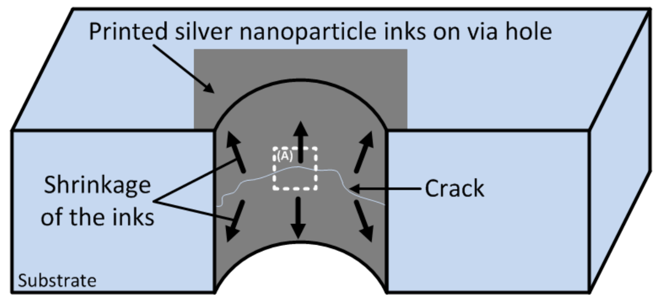

(a)

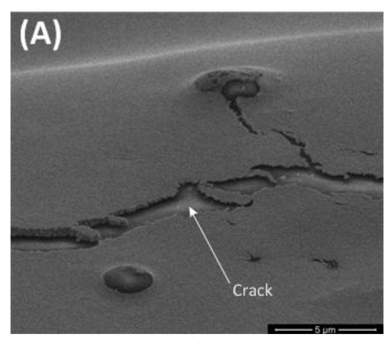

(b)

Fig. 5. (a) Crack formation of the inkjet-printed silver nanoparticle on a straight vertical via hole. (b) SEM image of the crack on the metalized via hole.

It is challenging to metalize via holes on relatively thick substrates. If the via holes are metalized with a similar approach to other inkjet-printed structures, i.e., printing multiple layers on drilled via holes, it results in discontinuities, as shown in Fig. 5. For demonstration purposes, a straight via hole was drilled on 1-mm-thick PMMA using CO_2 laser, and silver nanoparticles were printed over the via hole five times. The printed via hole was sintered at 120 °C for 1 h. The printed silver nanoparticles failed to form a continuous metal layer on the via hole because of the shrinkage of the silver ink during the sintering process due to the evaporation of the solvents, the polymers (a dispersant on the silver nanoparticles), and the impurities of the ink. The gravity force further enhances the downward shrinkage of the ink, which results in cracks on the metalized via wall. The shrinkage of the inkjet-printed silver nanoparticles on the vertical via wall is briefly shown in Fig. 5(a). The inkjet-printed silver nanoparticles on the vertical wall are shrinking in different directions, and these results in cracks, as shown in Fig. 5(b).

A novel stepped-via hole topology is introduced in order to create a gradual transition between the top and bottom planar substrate surfaces and reduce the stress on printed silver nanoparticles on the via hole during the sintering process. The fabrication process is described in Fig. 6. A thin concentric circular cylinder is engraved on the substrate to form a stepped-via profile [Fig. 6(a-i) and (a-ii)]. Then, the substrate is flipped to drill another stepped via on the bottom side [Fig. 6(a-iii) and (a-iv)]. It is necessary to form a smooth transition from the via top to the bottom of the substrate. The final step is the inkjet-printing process [Fig. 6(a-v) and (a-vi)]. The fabricated stepped-via hole on PMMA is shown in Fig. 6(b). This fabrication process is suitable for the inkjet printing, because the drilling process and the inkjet-printing process are completely separate, while the via metallization is easily achieved during the inkjet printing (totally dry) process without any additional steps. The fabrication concept shown here on the PMMA substrate is for the proof-of-concept only, and is equally applicable to any other inkjet-printable substrates.

The fabricated inkjet-printed vias are shown in Fig. 7 and Fig. 8. The geometries of the stepped via (top and side views) are shown in Figs. 7(a) and 8(a). Five concentric disks were drilled to form a stepped-via profile on the top, and two concentric disks were drilled on the bottom. A symmetric via profile (the same number of disks on the top and the bottom) requires the precise control of the laser power level and alignment to match each end of the drilled stepped-via topology, which is more significantly challenging than the asymmetric stepped-via topology. The ratio of the drilled disks is kept to the same value. The two concentric disks on the bottom with gradually increasing radii make sure that the penetration of the via hole runs through the entire substrate, because the upper five concentric disks with gradually decreasing radii sometime fail to form a through hole due to the misalignment of the laser focus or uneven substrate surface. The bottom disks also improve the metal continuity, because they enable a smoother transition from the via to the bottom by chamfering the transition from the via to the bottom layer. The disk radii of R_1 and R_2 are chosen for the bottom disks to facilitate the alignment and the fabrication, since misalignment and fabrication errors can be compensated within the larger radii R_1 and R_2. The equal via radii at the top and bottom via disks assist in the easier continuation of the layout at the top layer to the layout at the bottom layer. The radius of each circular disk is shown in Fig. 7(a),

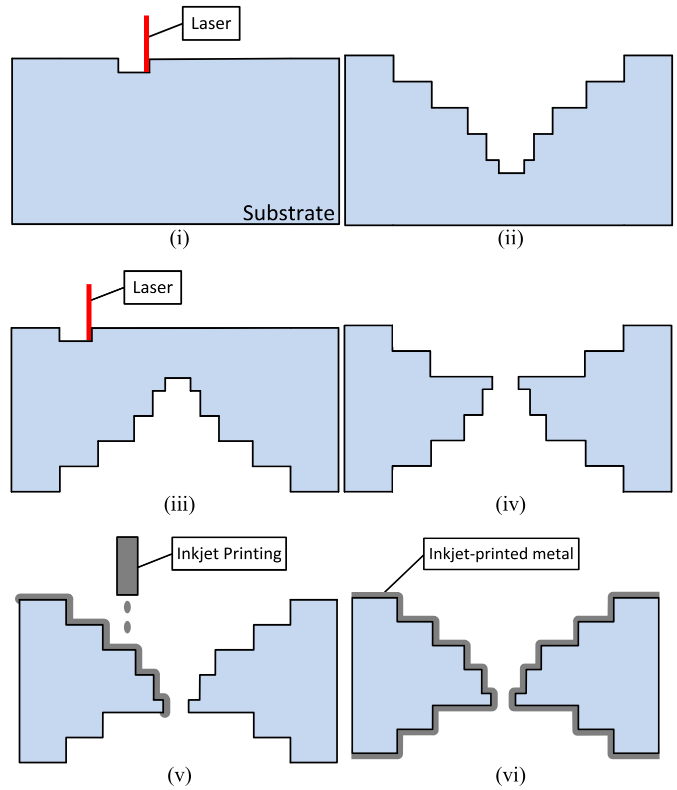

(a)

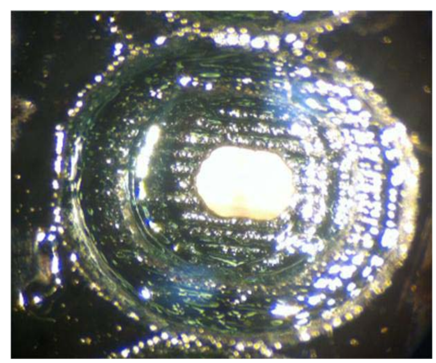

(b)

Fig. 6. (a) Stepped-via hole fabrication process. (a-i) Laser drilling (top). (a-ii) Drilled via hole (top). (a-iii) Laser drilling (bottom). (a-iv) Drilled-via hole (top and bottom). (a-v) Inkjet printing and sintering. (a-vi) Fabricated stepped-via hole. (b) Fabricated stepped-via hole (magnification ratio: 10×).

featuring exponentially tapered values ($r_{n+1} = e^{-1} \cdot r_n$). A universal laser system's PLS6.75 CO_2 laser was utilized. The laser was raster-scanned over the concentric circles at 1.4 W in a speed of 71 cm/s and a resolution of 1000 pulses per inch (PPI). Five layers of silver nanoparticle ink were printed over the engraved stepped-via hole using the same inkjet-printing machine and settings discussed in Section II-A. The printed via sample was sintered at 120 °C for 2 h. Scanning electron microscope (SEM) images are shown in Figs. 7(b) and 8(b). Quanta 3-D FEG SEM tool was utilized in this paper. Fig. 7(b)-A shows the semicircular area of the inkjet-printed stepped via, which corresponds to a dashed box in Fig. 7(a) (top view). The stepped profile of via is clearly observed with continuous metallization [Fig. 7(b)-A].

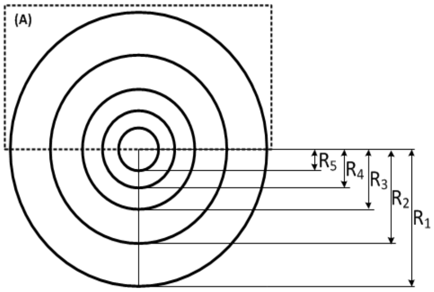

Radius	Value (mm)
R_1	1.00
R_2	0.63
R_3	0.40
R_4	0.25
R_5	0.16

(a)

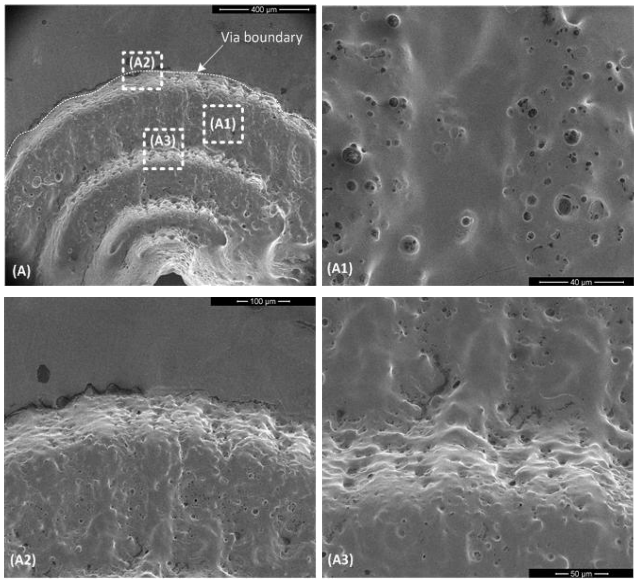

(b)

Fig. 7. (a) Geometry of stepped-via hole. (b) SEM images of the metalized stepped-via hole (top view).

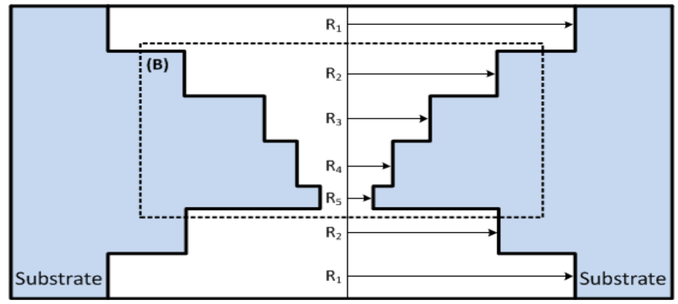

(a)

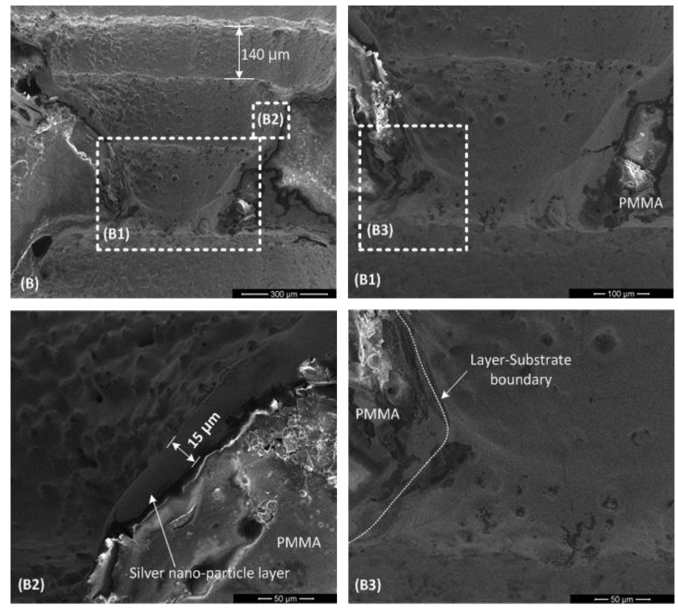

(b)

Fig. 8. (a) Geometry of stepped-via hole. (b) SEM images of the metalized stepped-via hole (side view).

Fig. 7(b)-A1–A3 shows the magnified SEM images of corresponding areas shown in Fig. 7(b)-A. Fig. 7(b)-A1 shows a planar area of the inkjet-printed stepped via. Fig. 7(b)-A2 shows the transition from the surface of the top substrate to the stepped via and Fig. 7(b)-A3 shows the transition between two consecutive stepped-via disks. The rough surface of the via hole is due to the laser raster scanning, which utilizes a pulse laser. The profile of the stepped-via hole is also shown in Fig. 8 (side view). Fig. 8(b)-B shows the area of the dashed boxes in Fig. 8(a). The depth of each step was $\sim$140 μm, and a continuous silver nanoparticle layer was observed throughout the entire stepped-via hole. Fig. 8(b)-B1–B3 shows the magnified SEM images of corresponding areas shown in Fig. 8(b)-B and B1. The silver nanoparticles form a solid layer along the via hole [Fig. 8(b)-B2 and B3], and a smooth transition from top to bottom is observed [Fig. 8(b)-B3]. The transition boundary between the silver nanoparticle layer and the PMMA substrate is shown in dashed line in Fig. 8(b)-B3. The proposed via fabrication process is compatible with the inkjet-printing technology as well as a cost-efficient process, since this process etches small volume of substrate material. A volume of seven-stepped-via hole shown in Figs. 7 and 8 is 1.03 mm^3, while a volume of a conventional cylindrical-via hole that has the same via radius of 1 mm is 3.14 mm^3. The equivalent radius of the conventional cylindrical-via hole that has the same etched volume is 0.57 mm.

A via chain that consisted of 5$\sim$40 inkjet-printed stepped vias was fabricated on 0.8-mm-thick Rogers RT/Duroid 5880, and the vias' dc resistance was measured to verify the repeatability and the robustness of the proposed fabrication process. The RT/Duroid 5880 was chosen to demonstrate the easy scalability of the proposed via topology, as it features low-loss tangent at gigahertz frequency range as well as high-temperature handling capability. The via chain was connected in a series. The measured resistances of the via arrays were 3.7 Ω for the 20 vias and 7.2 Ω for the 40 vias. The average resistance of the each inkjet-printed stepped via was $\sim$0.2 Ω, as shown in Fig. 9. The via resistances on PMMA and Rogers RT/Duroid 5880 are different because of substrate thickness and surface energy of the substrates. The thickness of RT/Duroid 5880 is 20% thinner than one of the PMMA. The RT/Duroid 5880 has higher surface energy than the PMMA resulting in thicker metal trace when silver nanoparticle ink is printed.

IV. Via Modeling

A typical cylindrical via can be modeled as an inductor and a resistor in series. Circuit models for a straight cylindrical via and for a generalized stepped via are shown in Fig. 10.

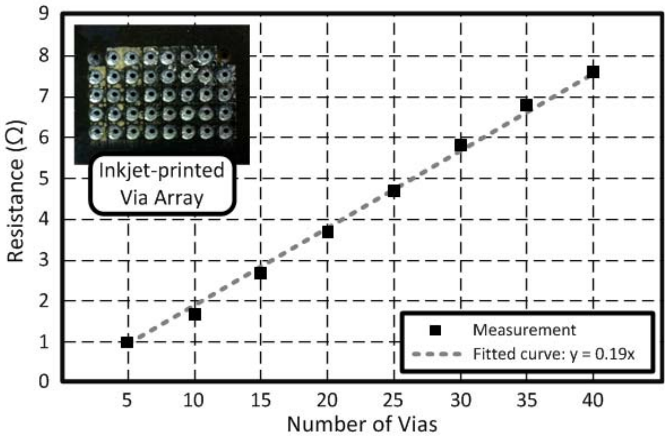

Fig. 9. Measured dc resistance of the via chain. Inset: inkjet-printed stepped-via array.

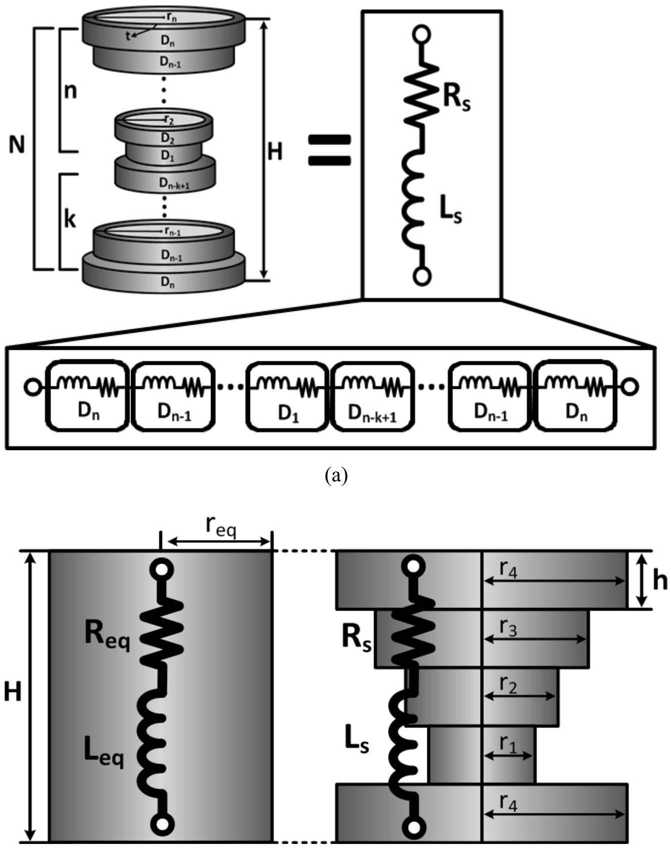

(a)

(b)

Fig. 10. (a) Equivalent circuit model of a stepped via. (b) Equivalent via model of a cylindrical via and a stepped via.

The proposed stepped via can be considered as a series of cylindrical vias [Fig. 10(a)], as shown in Fig. 10(b). The transition between the adjacent cylinders, such as D_2, D_1, and D_{n-k+1}, can be easily achieved when both the top and bottom sides are printed one by one, as discussed in Section III. The equivalent shunt capacitance of the stepped via is negligible when the length of the stepped via is much smaller than a wavelength at the operation frequency. For simplicity and without the loss of generality, the cylinder on the bottom is chosen to have the same dimensions with the cylinders on the top, as shown in Fig. 10(b), and their equivalent circuit model (an inductance value and a resistance value) is derived based on the geometry of the vias. An inductance value (L_{eq}) and a resistance value (R_{eq}) of a straight cylindrical via can be expressed, as shown in (3) and (4), where the radius of the cylindrical-via hole is r_{eq}, the metal thickness is t, and the height of the via is H

$$\begin{cases} L_{\text{eq}} = \dfrac{\mu_0 H}{4\pi} f(r_{\text{eq}}, t) \\ R_{\text{eq}} = \dfrac{H}{\sigma\pi} g(r_{\text{eq}}, t) \end{cases} \tag{3}$$

where

$$\begin{cases} f(r_{\text{eq}}, t) = \dfrac{r_{\text{eq}}^2 - (r_{\text{eq}} - t)^2 - 2(r_{\text{eq}} - t)^2 \ln\left(\frac{r_{\text{eq}}}{r_{\text{eq}} - t}\right)}{r_{\text{eq}}^2 - (r_{\text{eq}} - t)^2} \\ g(r_{\text{eq}}, t) = \dfrac{1}{t(2r_{\text{eq}} - t)}. \end{cases} \tag{4}$$

Similarly, the circuit model (L_s and R_s) of the proposed stepped-via hole can be derived based on (3) and (4), as shown in

$$\begin{cases} L_s = \frac{\mu_0 \text{h}}{4\pi}\left[2\sum\limits_{i=1}^{n} f(r_i, t) + \sum\limits_{i=n-k+1}^{n} f(r_i, t)\right] \\ R_s = \frac{1}{\sigma\pi}\left[h\left(\sum\limits_{i=1}^{n} g(r_i, t) + \sum\limits_{i=n-k+1}^{n} g(r_i, t)\right)\right. \\ \qquad\qquad \left. + \sum\limits_{i=1}^{n-1} h(r_{i+1}, r_i, t) + \sum\limits_{i=n-k+1}^{n-1} h(r_{i+1}, r_i, t)\right] \end{cases}$$
$$(N = n + k,\ k \geq 1) \tag{5}$$

$$\begin{cases} f(r_i, t) = \dfrac{r_i^2 - (r_i - t)^2 - 2(r_i - t)^2 \ln(\frac{r_i}{r_i - t})}{r_i^2 - (r_i - t)^2} \\ g(r_i, t) = \dfrac{1}{t(2r_i - t)} \\ h(r_{i+1}, r_i, t) = \dfrac{t}{(r_{i+1} - t)^2 - (r_i - t)^2}. \end{cases} \tag{6}$$

The performance of the inkjet-printed via, such as the cutoff frequency, the inductance, and the resistance of the printed via, is a strong function of the via radius based on (5) and (6). A via segment with a smallest radius is the most important segment of the proposed stepped-via topology, since the inductance increases exponentially as the radius decreases, while the resistance is inversely proportional to the via radius.

The proposed stepped-via topology is easy to fabricate utilizing the inkjet-printing technology, but it is impractical to model every different stepped-via topologies in full-wave 3-D simulators, such as HFSS and Computer Simulation Technology. It is convenient to derive an effectively equivalent straight cylindrical via circuit model, where the composite inductance and resistance values are the same with the proposed stepped via. The five-layered stepped via was assumed on 0.8-mm-thick RT/Duroid 5880, as shown in Fig. 10, as a design example. The height of each cylinder (h) was 200 μm, the radius of the largest cylinder (r_4) was 1 mm, and the metal thickness (t) was set to 210 nm with a conductivity value of 9×10^6 S/m.

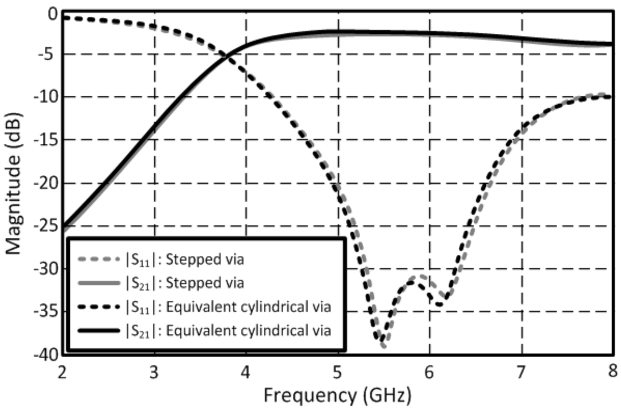

Fig. 11. Simulated S-parameters of the SIW structure with a stepped-via topology and an equivalent cylindrical-via topology.

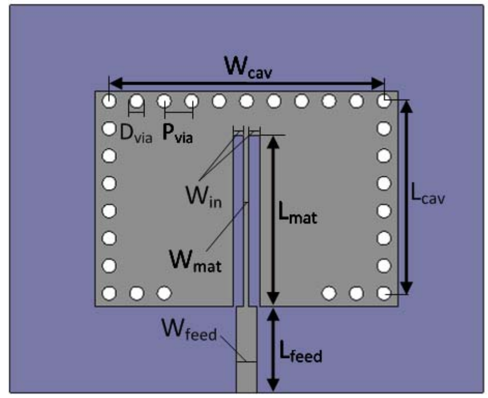

Fig. 12. Geometry of the SIW cavity resonator. $W_{\text{feed}} = 2.5$ mm. $L_{\text{feed}} = 10$ mm. $W_{\text{cav}} = 32$ mm. $L_{\text{cav}} = 22.4$ mm. $D_{\text{via}} = 1.6$ mm. $P_{\text{via}} = 3.2$ mm. $L_{\text{mat}} = 17$ mm. $W_{\text{mat}} = 0.6$ mm. $W_{\text{in}} = 1.25$ mm.

The radii were exponentially increased ($r_{n+1} = e \cdot r_n$). The equivalent circuit model (L_{eq} and R_{eq}) of a cylindrical via was designed based on (3)–(6). The equivalent radius (r_{eq}) of a cylindrical via was 360 μm with a metal thickness of 180 nm and a conductivity value of 1×10^7 S/m. Each value was calculated from the proposed equations (3)–(6). The designed equivalent circuit model of the cylindrical via has the same inductance and resistance with those values of the stepped via ($L_{\text{eq}} = L_s = 45.28$ pH and $R_{\text{eq}} = R_s = 0.2\ \Omega$). The resistance value agrees with the measurement shown in Fig. 9. The simulated equivalent via and stepped-via models at microwave frequency band are shown in Fig. 11, and the results agree very well.

V. Inkjet-Printed SIW Components

An SIW technology is one of the most promising technologies for high-frequency applications, and numerous studies have been reported at the microwave frequency band [19]. However, there are not many reported works on printed SIW components, including via metallization methods, using a printing technology. The results of the inkjet-printed stepped vias and the substrate characterization at microwave frequency range suggest that the relatively high conductivity values of inkjet-printed silver nanoparticles ($4.6 \times 10^6 \sim 8 \times 10^6$ S/m) and fabrication of numerous vias can be easily achieved. As a proof of the via fabrication concept and its application, various SIW components with large number of vias were designed, and the prototypes were experimentally investigated. Therefore, in this paper, SIW structures are chosen as a design example utilizing the proposed stepped-via topology to implement fully printed SIW components. In this section, a microstrip-to-SIW transition and an SIW cavity resonator are presented.

A. SIW Cavity Resonator

An inkjet-printed SIW cavity resonator has been designed to verify the performance of the inkjet-printed vias. The cavity was designed to resonate at 5.8 GHz on 0.8-mm-thick Rogers RT/Duroid 5880 ($\varepsilon_r = 2.2$ and $\tan\delta = 0.0009$ at 10 GHz) in order to minimize the effect of substrate loss. The geometry of the designed SIW cavity is shown in Fig. 12. The top and bottom sides of the substrate were drilled utilizing a laser to form a stepped-via profile, as discussed in Section III. The designed pattern was printed five layers on the top side, and a 45 mm × 40 mm patch was printed on the bottom side as a ground plane.

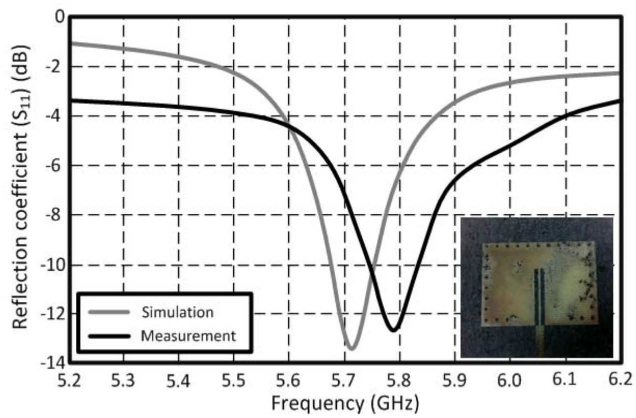

Fig. 13. Simulated and measured reflection coefficient (S_{11}) of the inkjet-printed SIW cavity resonator.

The measured and simulated reflection coefficients (S_{11}) are shown in Fig. 13. The results match reasonably well, and their small discrepancy is due to fabrication errors stemming from the dispersion of ink on substrate after printing. The quality factor (Q-factor) of the fabricated SIW cavity is calculated using

$$Q = \frac{f_r}{\Delta f_{3\text{dB}}} \tag{7}$$

where f_r is the resonant frequency and $\Delta f_{3\text{dB}}$ is the 3-dB bandwidth (half power bandwidth). The measured resonant frequency was 5.79 GHz, and the 3-dB bandwidth was 0.23 GHz, which results in a Q-factor of 25.13, while the simulated Q-factor was 20.05 at 5.73 GHz. The achieved Q-factor of the inkjet-printed SIW cavity was relatively low compared with the conventional cavity resonators [33], [34], since the inkjet-printed metallic layer has thin metal thickness (<5 μm) and a relatively low conductivity value compared with a bulk copper ($\sigma_{\text{printed}} = 9 \times 10^6$ S/m and $\sigma_{\text{cu}} = 5.96 \times 10^7$ S/m) resulting in a high loss from metal layers.

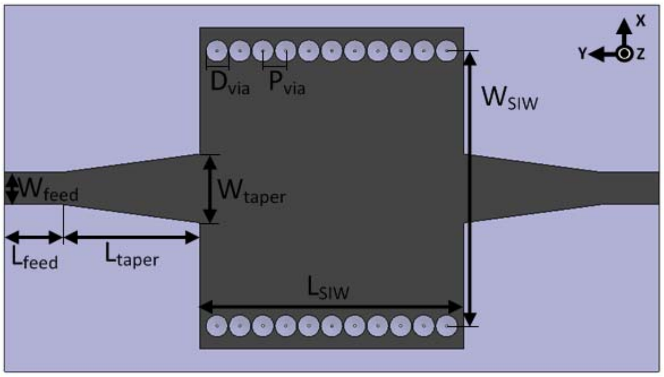

(a)

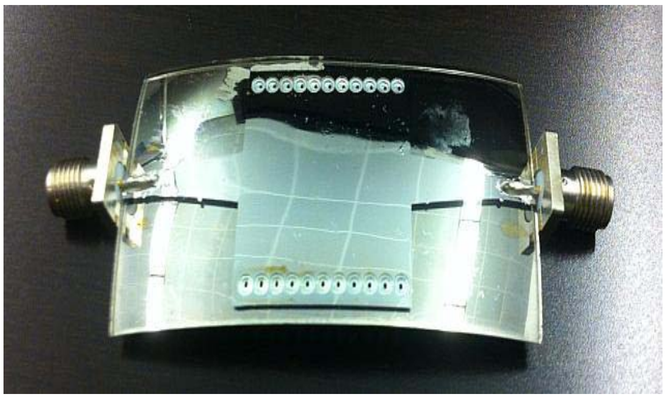

(b)

Fig. 14. Microstrip-to-SIW transition. (a) Geometry: $W_{\text{feed}} = 2.8$ mm, $W_{\text{taper}} = 6$ mm, $L_{\text{SIW}} = 23$ mm, $W_{\text{SIW}} = 24$ mm, $D_{\text{via}} = 2$ mm, $P_{\text{via}} = 2$ mm, $L_{\text{feed}} = 5$ mm, and $L_{\text{taper}} = 12$ mm. (b) Fabricated component on PMMA.

B. Inkjet-Printed Microstrip-to-SIW Transition

A simple microstrip-to-SIW transition on PMMA has been designed, and it was fully inkjet-printed by utilizing the stepped-via structure for the first time. Its fundamental mode cutoff frequency (f_0) has been set to 4 GHz in order to enable an operating frequency of 5 GHz. The geometry of the proposed microstrip-to-SIW transition is shown in Fig. 14(a). Each corner of PMMA was bent due to the thermal expansion of the substrate, but the middle of the SIW was flat. The SIW and the tapered transition were designed and optimized by following the reported design guide described in [35] and [36]. The width (W_{SIW}) and the length (L_{SIW}) of the SIW were 24 and 23 mm, respectively. The diameter (D_{via}) and the pitch (P_{via}) of the stepped vias were both equal to 2 mm. The length (L_{taper}) of the tapered microstrip-to-SIW transition was 12 mm, and the width (W_{taper}) of it was 6 mm. The thickness of the substrate is 1 mm. Fig. 14(b) shows the fully inkjet-printed microstrip-to-SIW transition on PMMA. Vias were drilled as introduced in Section III, and then, the SIW pattern and the ground plane were printed. The printer settings and the sintering temperature were the same, as presented in Section II-A.

The measured and simulated values of the magnitude of the scattering parameters ($|S_{11}|$ and $|S_{21}|$) are shown in Fig. 15, demonstrating good agreement. The measured insertion loss

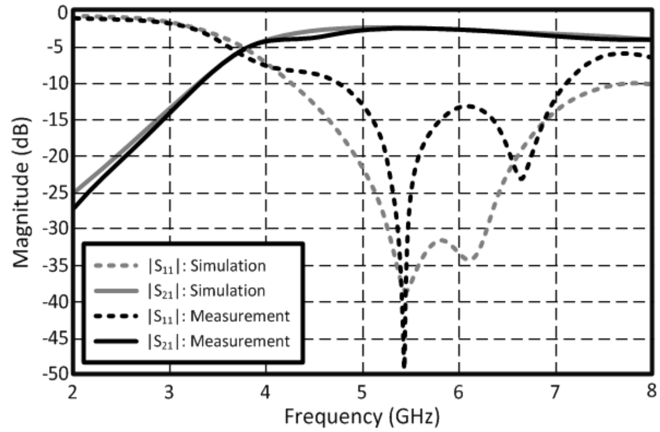

Fig. 15. Measured scattering parameters of microstrip-to-SIW transition.

of the proposed microstrip-to-SIW at 5 GHz is 2.4 dB. It is notable that the inkjet-printed vias have been successfully implemented.

VI. Conclusion and Future Work

In this paper, the inkjet-printing process of silver nanoparticles on thick substrates, such as a PMMA and RT/Duroid 5880, for microwave applications as well as the fabrication process of fully inkjet-printed low-cost vias and SIW components is demonstrated. The inkjet-printed silver nanoparticle inks on PMMA feature good conductivity values ($4.5 \times 10^6 \sim 8 \times 10^6$ S/m) to implement practical microwave topologies. The fully inkjet-printed vias on the PMMA substrate were implemented by introducing a novel stepped-via hole configuration with an exponentially tapered radial profile. As a proof-of-concept, fully inkjet-printed SIW structures, such as an SIW cavity resonator and a microstrip-to-SIW transition, were designed and experimentally demonstrated, verifying the feasibility of inkjet-printed stepped vias on various substrates.

The work presented in this paper is a fundamental study toward the future fully inkjet-printed low-cost via-enabled devices and systems, including packaging. The next step of this paper is to increase the thickness of the inkjet-printed silver nanoparticle films in order to reduce the skin depth effect. A proper surface treatment, such as the modification of the surface energy (surface functionalization or ozone treatment), and applying mechanical constraints (increase surface roughness or implement channel for the inks) [37], could improve the printable thickness, adhesion, and uniformity of silver nanoparticles.

References

[1] L. Atzori, A. Iera, and G. Morabito, "The Internet of Things: A survey," *Comput. Netw.*, vol. 54, no. 15, pp. 2787–2805, Oct. 2010.

[2] V. Lakafosis, A. Rida, R. Vyas, L. Yang, S. Nikolaou, and M. M. Tentzeris, "Progress towards the first wireless sensor networks consisting of inkjet-printed, paper-based RFID-enabled sensor tags," *Proc. IEEE*, vol. 98, no. 9, pp. 1601–1609, Sep. 2010.

[3] M. Singh, H. M. Haverinen, P. Dhagat, and G. E. Jabbour, "Inkjet printing—Process and its applications," *Adv. Mater.*, vol. 22, no. 6, pp. 673–685, Feb. 2010.

[4] P. Calvert, "Inkjet printing for materials and devices," *Chem. Mater.*, vol. 13, no. 10, pp. 3299–3305, Sep. 2001.

[5] L. Yang, A. Rida, R. Vyas, and M. M. Tentzeris, "RFID tag and RF structures on a paper substrate using inkjet-printing technology," *IEEE Trans. Microw. Theory Techn.*, vol. 55, no. 12, pp. 2894–2901, Dec. 2007.

[6] M. Mantysalo *et al.*, "Evaluation of inkjet technology for electronic packaging and system integration," in *Proc. 57th IEEE Electron. Compon. Technol. Conf.*, Reno, NV, USA, May/Jun. 2007, pp. 89–94.

[7] J.-U. Park *et al.*, "High-resolution electrohydrodynamic jet printing," *Nature Mater.*, vol. 6, pp. 782–789, Aug. 2007.

[8] M. F. Mabrook, C. Pearson, and M. C. Petty, "Inkjet-printed polymer films for the detection of organic vapors," *IEEE Sensors J.*, vol. 6, no. 6, pp. 1435–1444, Dec. 2006.

[9] K. Kordás *et al.*, "Inkjet printing of electrically conductive patterns of carbon nanotubes," *Small*, vol. 2, nos. 8–9, pp. 1021–1025, Aug. 2006.

[10] S. M. Z. Hossain *et al.*, "Development of a bioactive paper sensor for detection of neurotoxins using piezoelectric inkjet printing of sol–gel-derived bioinks," *Anal. Chem.*, vol. 81, pp. 5474–5483, Jun. 2009.

[11] T. Kaydanova, A. Miedaner, J. D. Perkins, C. Curtis, J. L. Alleman, and D. S. Ginley, "Direct-write inkjet printing for fabrication of barium strontium titanate-based tunable circuits," *Thin Solid Films*, vol. 515, nos. 7–8, pp. 3820–3824, Feb. 2007.

[12] S. Kim, A. Georgiadis, A. Collado, and M. M. Tentzeris, "An inkjet-printed solar-powered wireless beacon on paper for identification and wireless power transmission applications," *IEEE Trans. Microw. Theory Techn.*, vol. 60, no. 12, pp. 4178–4186, Dec. 2012.

[13] S. Kim *et al.*, "Inkjet-printed antennas, sensors and circuits on paper substrate," *IET Microw. Antennas Propag.*, vol. 7, no. 10, pp. 858–868, Jul. 2013.

[14] I. Reinhold, M. Thielen, W. Voit, W. Zapka, R. Gotzen, and H. Bohlmann, "Inkjet printing of electrical vias," in *Proc. 18th Eur. Microelectron. Packag. Conf.*, Brighton, U.K., Sep. 2011, pp. 1–4.

[15] T. Kawase, H. Sirringhaus, R. H. Friend, and T. Shimoda, "Inkjet printed via-hole interconnections and resistors for all-polymer transistor circuits," *Adv. Mater.*, vol. 13, no. 21, pp. 1601–1605, Nov. 2001.

[16] T. Falat, J. Felba, A. Moscicki, and J. Borecki, "Nano-silver inkjet printed interconnections through the microvias for flexible electronics," in *Proc. 11th IEEE Conf. Nanotechnol.*, Portland, OR, USA, Aug. 2011, pp. 473–477.

[17] G. McKerricher, J. Gonzalez, and A. Shamim, "All inkjet printed 3D microwave capacitors and inductors with vias," in *IEEE MTT-S Int. Microw. Symp. Dig.*, Seattle, WA, USA, Jun. 2013, pp. 1–3.

[18] B. K. Tehrani, J. Bito, B. S. Cook, and M. M. Tentzeris, "Fully inkjet-printed multilayer microstrip and T-resonator structures for the RF characterization of printable materials and interconnects," in *IEEE MTT-S Int. Microw. Symp. Dig.*, Tampa, FL, USA, Jun. 2014, pp. 1–4.

[19] M. Bozzi, A. Georgiadis, and K. Wu, "Review of substrate-integrated waveguide circuits and antennas," *IET Microw. Antenna Propag.*, vol. 5, no. 8, pp. 909–920, Jun. 2011.

[20] R. Moro, S. Kim, M. Bozzi, and M. M. Tentzeris, "Inkjet-printed paper-based substrate-integrated waveguide (SIW) components and antennas," *Int. J. Microw. Wireless Technol.*, vol. 5, no. 3, pp. 197–204, May 2013.

[21] Y. N. Srivastava *et al.*, "Polymethylmethacrylate membrane for fluid encapsulation and release in microfluidic systems," *J. Vac. Sci. Technol. A*, vol. 22, no. 3, pp. 1067–1072, May 2004.

[22] K.-P. Latti, M. Kettunen, J.-P. Strom, and P. Silventoinen, "A review of microstrip T-resonator method in determining the dielectric properties of printed circuit board materials," *IEEE Trans. Instrum. Meas.*, vol. 56, no. 5, pp. 1845–1850, Oct. 2007.

[23] Y. Son, C. Kim, D. H. Yang, and D. J. Ahn, "Spreading of an inkjet droplet on a solid surface with a controlled contact angle at low Weber and Reynolds numbers," *Langmuir*, vol. 24, no. 6, pp. 2900–2907, Feb. 2008.

[24] *Goodfellow*. [Online]. Available: http://www.goodfellow.com/, accessed Feb. 4, 2016.

[25] D. Soltman and V. Subramanian, "Inkjet-printed line morphologies and temperature control of the coffee ring effect," *Langmuir*, vol. 24, no. 5, pp. 2224–2231, Jan. 2008.

[26] T. H. J. van Osch, J. Perelaer, A. W. M. de Laat, and U. S. Schubert, "Inkjet printing of narrow conductive tracks on untreated polymeric substrates," *Adv. Mater.*, vol. 20, no. 2, pp. 343–345, Jan. 2008.

[27] J. Perelaer, B.-J. de Gans, and U. S. Schubert, "Ink-jet printing and microwave sintering of conductive silver tracks," *Adv. Mater.*, vol. 18, no. 16, pp. 2101–2104, Aug. 2006.

[28] S. Kim *et al.*, "No battery required: Perpetual RFID-enabled wireless sensors for cognitive intelligence applications," *IEEE Microw. Mag.*, vol. 14, no. 5, pp. 66–77, Jul./Aug. 2013.

[29] J. Perelaer, C. E. Hendriks, A. W. M. de Laat, and U. S. Schubert, "One-step inkjet printing of conductive silver tracks on polymer substrates," *Nanotechnology*, vol. 20, no. 16, p. 165303, Mar. 2009.

[30] R. A. Pucel, D. J. Masse, and C. P. Hartwig, "Losses in microstrip," *IEEE Trans. Microw. Theory Techn.*, vol. 16, no. 6, pp. 342–350, Jun. 1968.

[31] F. Declercq, H. Rogier, and C. Hertleer, "Permittivity and loss tangent characterization for garment antennas based on a new matrix-pencil two-line method," *IEEE Trans. Antennas Propag.*, vol. 56, no. 8, pp. 2548–2554, Aug. 2008.

[32] H.-Y. Ko, J. Park, H. Shin, and J. Moon, "Rapid self-assembly of monodisperse colloidal spheres in an ink-jet printed droplet," *Chem. Mater.*, vol. 16, no. 22, pp. 4212–4215, Oct. 2004.

[33] A. Collado, F. Mira, and A. Georgiadis, "Mechanically tunable substrate integrated waveguide (SIW) cavity based oscillator," *IEEE Microw. Wireless Compon. Lett.*, vol. 23, no. 9, pp. 489–491, Sep. 2013.

[34] J. D. Martinez, S. Sirci, M. Taroncher, and V. E. Boria, "Compact CPW-fed combline filter in substrate integrated waveguide technology," *IEEE Microw. Wireless Compon. Lett.*, vol. 22, no. 1, pp. 7–9, Jan. 2012.

[35] D. Deslandes and K. Wu, "Accurate modeling, wave mechanisms, and design considerations of a substrate integrated waveguide," *IEEE Trans. Microw. Theory Techn.*, vol. 54, no. 6, pp. 2516–2526, Jun. 2006.

[36] D. Deslandes, "Design equations for tapered microstrip-to-substrate integrated waveguide transitions," in *IEEE MTT-S Int. Microw. Symp. Dig.*, May 2010, pp. 704–707.

[37] C. E. Hendriks, P. J. Smith, J. Perelaer, A. M. J. van de Berg, and U. S. Schubert, "'Invisible' silver tracks produced by combining hot-embossing and inkjet printing," *Adv. Funct. Mater.*, vol. 18, no. 7, pp. 1031–1038, Apr. 2008.

Sangkil Kim (S'12–M'15) received the B.S. degree in electrical and electronic engineering from Yonsei University, Seoul, Korea, in 2010, and the M.S. and Ph.D. degrees in electrical and computer engineering from the Georgia Institute of Technology, Atlanta, GA, USA, in 2012 and 2014, respectively.

He is currently with Qualcomm, San Diego, CA, USA, where he is involved in the design and analysis of inductors/transformers for high power CMOS power amplifier and Low Noise Amplifier modules for wireless communication applications.

Atif Shamim (S'03–M'09–SM'13) received the M.A.Sc. and Ph.D. degrees in electrical engineering from Carleton University, Ottawa, ON, Canada, in 2004 and 2009, respectively.

He was an Invited Researcher with the VTT Micro-Modules Research Center, Oulu, Finland, in 2006. He was an NSERC Alexander Graham Bell Graduate Scholar with Carleton University from 2007 to 2009, and an NSERC Post-Doctoral Fellow with the Royal Military College of Canada, Kingston, ON, Canada, and the King Abdullah University of Science and Technology (KAUST), Thuwal, Saudi Arabia, from 2009 to 2010. In 2010, he joined the Electrical Engineering Program, KAUST, where he is currently an Assistant Professor and a Principle Investigator of the IMPACT Laboratory. He has authored or co-authored over 100 international publications and holds 13 patents. His current research interests include integrated on-chip antennas, low-power CMOS Radio Frequency Integrated Circuits for system-on-chip applications, and advanced system-on-package designs in multilayer Low Temperature Co-fired Ceramic, Liquid Crystal Polymer, and paper substrates through screen and inkjet printing techniques.

Dr. Shamim was a recipient of the Best Paper Prize at the European Wireless Technology Conference in 2008. He received the Ottawa Centre of Research Innovation (OCRI) Researcher of the Year Award in 2008. His work on wireless dosimeter won the ITAC SMC Award at Canadian Microelectronics Corporation TEXPO, Queen's University, Kingston, ON, Canada, in 2007. He received the Best Student Paper Finalist Prize at the IEEE Antennas and Propagation Society in 2005. He also won numerous business related awards, including first prize in Canada's National Business Plan Competition, and was selected for the OCRI Entrepreneur of the Year Award in 2010.

Apostolos Georgiadis (S'94–M'03–SM'08) was born in Thessaloniki, Greece. He received the Ph.D. degree in electrical engineering from the University of Massachusetts at Amherst, Amherst, MA, USA, in 2002.

He joined the Centre Tecnologic de Telecomunicacions de Catalunya (CTTC), Barcelona, Spain, as a Senior Researcher, in 2007, where he is involved in energy harvesting and radio-frequency identification (RFID) technology and active antennas and antenna arrays. Since 2013, he has been coordinating the Microwave Systems and Nanotechnology Department with CTTC.

Dr. Georgiadis was the Chair of the 2011 IEEE RFID Technologies and Applications Conference. He was also the Chair of EU COST Action IC0803: RF/Microwave Communication Subsystems for Emerging Wireless Technologies. He is the Vice Chair of EU COST Action IC1301 on Wireless Power Transfer for Sustainable Electronics. He serves as an Associate Editor of the IEEE MICROWAVE WIRELESS COMPONENTS LETTERS, the IEEE RFID VIRTUAL JOURNAL, and *IET Microwaves, Antennas and Propagation*. He was the Chair of the IEEE Microwave Theory and Technique (MTT) Society Technical Committee MTT-24 on RFID Technologies and a member of the IEEE MTT-26 on Wireless Energy Transfer and Conversion. He is the Vice Chair of the URSI Commission D Electronics and Photonics and a Distinguished Lecturer of the IEEE Council on RFID.

Hervé Aubert (M'94–SM'99) was born in Toulouse, France, in 1966. He received the Dipl.-Ing. and Ph.D. (Hons.) degrees in electrical engineering from the Institut National Polytechnique de Toulouse (INPT), Toulouse, in 1989 and 1993, respectively.

He was a Visiting Associate Professor with the School of Engineering and Applied Science, University of Pennsylvania, Philadelphia, PA, USA, from 1997 to 1998. He has been a Professor with INPT since 2001. He joined the Laboratory for Analysis and Architecture of Systems (LAAS), National Center for Scientific Research (CNRS), Toulouse, in 2006. Since 2015, he has been the Head of the Micro- and Nano-Systems for Wireless Communications Research Group with LAAS-CNRS. He was the Co-Chairman of the Electronics Laboratory with INPT from 2001 to 2005, and the Head of the Electromagnetics Research Group with the Electronics Laboratory from 2002 to 2005. He has performed research work on integral-equation and variational methods applied to electromagnetic wave propagation and scattering. He has authored or co-authored one book, two book chapters, 75 papers in refereed journals, and 200 communications in international symposium proceedings. His current research interests include the electromagnetic modeling of complex (multi-scale) structures and wireless sensors networks.

Dr. Aubert is a member of the Editorial Board of the *International Journal of Microwave Science and Technology* and the *International Journal of Antennas and Propagation*. He serves as an Associate Editor of *Electronics Letters*. He was the General Chairman of the European Microwave Week, Paris, France, in 2015. He has been an Expert for the French National Research Agency since 2009, and the European Commission since 2012.

Manos M. Tentzeris (S'89–M'92–SM'03–F'10) received the Diploma (*magna cum laude*) degree in electrical and computer engineering from the National Technical University of Athens, Athens, Greece, and the M.S. and Ph.D. degrees in electrical engineering and computer science from the University of Michigan, Ann Arbor, MI, USA.

He was a Visiting Professor with the Technical University of Munich, Munich, Germany, in 2002, Georgia Tech Ireland, Athlone, Ireland, in 2009, and the Laboratory for Analysis and Architecture of Systems–National Center for Scientific Research, Toulouse, France, in 2010. He served as the Head of the GT-ECE Electromagnetics Technical Interest Group, the NSF-Packaging Research Center Associate Director of RF Research and the RF Alliance Leader of the Georgia Institute of Technology (Georgia Tech), Atlanta, GA, USA, from 2003 to 2006, and the Georgia Electronic Design Center Associate Director of RFID/Sensors Research from 2006 to 2010. He has helped develop academic programs in highly integrated/multilayer packaging for radio frequency (RF) and wireless applications using ceramic and organic flexible materials, paper-based radio-frequency identifications (RFIDs) and sensors, biosensors, wearable electronics, 3-D/4-D/inkjet-printed electronics, green electronics, energy harvesting and wireless power transfer systems, Near Field Communication systems, nanotechnology applications in RF, origami-folded electromagnetics, microwave microelectromechanical systems, and system-on-package-integrated (Ultra Wide Band, multiband, millimeter wave, and conformal) antennas, and heads the ATHENA Research Group, Atlanta, GA, USA (20 researchers). He has given more than 100 invited talks to various universities and companies all over the world. He is currently a Professor with the School of Electrical and Computer Engineering, Georgia Tech. He has authored over 600 papers in refereed journals and conference proceedings, five books, and 24 book chapters.

Dr. Tentzeris is a member of the URSI-Commission D, the Microwave Theory and Technique (MTT)-15 Committee, and the Technical Chamber of Greece, an Associate Member of the European Microwave Association, and a fellow of the Electromagnetic Academy. He was a recipient/co-recipient of the 2015 IET Microwaves, Antennas and Propagation Premium Award, the 2014 Georgia Tech ECE Distinguished Faculty Achievement Award, the 2014 IEEE RFID Technologies and Applications Conference Best Student Paper Award, the 2013 IET Microwaves, Antennas and Propagation Premium Award, the 2012 FiDiPro Award in Finland, the iCMG Architecture Award of Excellence, the 2010 IEEE Antennas and Propagation Society (APS) Piergiorgio L. E. Uslenghi Letters Prize Paper Award, the 2011 International Workshop on Structural Health Monitoring Best Student Paper Award, the 2010 Georgia Tech Senior Faculty Outstanding Undergraduate Research Mentor Award, the 2009 IEEE TRANSACTIONS ON COMPONENTS AND PACKAGING TECHNOLOGIES Best Paper Award, the 2009 E.T.S. Walton Award from the Irish Science Foundation, the 2007 IEEE APS Symposium Best Student Paper Award, the 2007 IEEE International Microwave Symposium (IMS) Third Best Student Paper Award, the 2007 International Symposium on Antennas and Propagation Poster Presentation Award, the 2006 IEEE MTT Outstanding Young Engineer Award, the 2006 Asian-Pacific Microwave Conference Award, the 2004 IEEE TRANSACTIONS ON ADVANCED PACKAGING Commendable Paper Award, the 2003 NASA Godfrey Art Anzic Collaborative Distinguished Publication Award, the 2003 IBC International Educator of the Year Award, the 2003 IEEE Components, Packaging, and Manufacturing Technology (CPMT) Outstanding Young Engineer Award, the 2002 International Conference on Microwave and Millimeter-Wave Technology Best Paper Award in Beijing, China, the 2002 Georgia Tech-ECE Outstanding Junior Faculty Award, the 2001 Applied Computational Electromagnetic Society Conference Best Paper Award, the 2000 NSF CAREER Award, and the 1997 Best Paper Award of the International Hybrid Microelectronics and Packaging Society. He was the TPC Chair of the IEEE IMS in 2008, and the Chair of the IEEE Workshop on Computational Electromagnetics in Time-Domain in 2005. He is the Vice Chair of the RF Technical Committee (TC16) of the IEEE CPMT Society. He is the Founder and Chair of the RFID Technical Committee (TC24) of the IEEE MTT Society and the Secretary/Treasurer of the IEEE Council on RFID (C-RFID). He is an Associate Editor of the IEEE TRANSACTIONS ON MICROWAVE THEORY AND TECHNIQUES, the IEEE TRANSACTIONS ON ADVANCED PACKAGING, and the *International Journal on Antennas and Propagation*. He served as one of the IEEE MTT Society Distinguished Microwave Lecturers from 2010 to 2012. He serves as one the IEEE C-RFID Distinguished Lecturers.